Journal of Complex Networks (2019) **7**, 932–960
doi: 10.1093/comnet/cnz013
Advance Access Publication on 15 April 2019

Effect of antipsychotics on community structure in functional brain networks

RYAN FLANAGAN AND LUCAS LACASA
School of Mathematical Sciences, Queen Mary University of London, London E1 4NS, UK

EMMA K. TOWLSON
Center for Complex Network Research and Department of Physics, Northeastern University, Boston, MA 02115, USA and Media Laboratory, Massachusetts Institute of Technology, Cambridge, MA 02139, USA

SANG HOON LEE
Department of Liberal Arts, Gyeongnam National University of Science and Technology, Jinju 52725, Korea

AND

MASON A. PORTER[†]
Department of Mathematics, University of California, Los Angeles, CA 90095, USA
[†]Corresponding author. Email: mason@math.ucla.edu

Edited by: Danielle Bassett

[Received on 1 June 2018; editorial decision on 21 February 2019; accepted on 23 February 2019]

Schizophrenia, a mental disorder that is characterized by abnormal social behaviour and failure to distinguish one's own thoughts and ideas from reality, has been associated with structural abnormalities in the architecture of functional brain networks. In this article, we (1) investigate whether mesoscale network properties give relevant information to distinguish groups of patients from controls in different scenarios and (2) use this lens to examine network effects of different antipsychotic treatments. Using various methods of network analysis, we examine the effect of two classical therapeutic antipsychotics—Aripiprazole and Sulpiride—on the architecture of functional brain networks of both controls (i.e., a set of people who were deemed to be healthy) and patients (who were diagnosed with schizophrenia). We compare community structures of functional brain networks of different individuals using mesoscopic response functions, which measure how community structure changes across different scales of a network. Our approach does a reasonably good job of distinguishing patients from controls, and the distinction is sharper for patients and controls who have been treated with Aripiprazole. Unexpectedly, we find that this increased separation between patients and controls is associated with a change in the control group, as the functional brain networks of the patient group appear to be predominantly unaffected by this drug. This suggests that Aripiprazole has a significant and measurable effect on community structure in healthy individuals but not in individuals who are diagnosed with schizophrenia, something that conflicts with the naive assumption that the drug alters the mesoscale network properties of the patients (rather than the controls). By contrast, we are less successful at separating the networks of patients from those of controls when the subjects have been given the drug Sulpiride. Taken together, in our results, we observe differences in the effects of the drugs (and a placebo) on community structure in patients and controls and also that this effect differs across groups. From a network-science perspective, we thereby demonstrate that different types of antipsychotic drugs selectively affect mesoscale properties of brain networks, providing support that structures such as communities are meaningful functional units in the brain.

Keywords: structural analysis of networks; brain networks; mathematical analysis of networks; community structure.

1. Introduction

Investigating the structure and dynamics of neuronal networks is crucial for understanding the human brain, and the nascent field of 'network neuroscience' has yielded fascinating insights into a diverse variety of neurological phenomena [1, 2]. Recent advances in imaging technology have made it possible to perform increasingly detailed investigations of brain structure and dynamics, and it is now possible to map anatomical regions and their interconnecting pathways at near-millimetre resolution. This yields large-scale networks with which to describe the brain's structural connectivity (i.e., the human connectome) [3, 4]. These structural connections have a crucial influence on large-scale neuronal dynamics, which can be captured as patterns of functional connectivity in so-called 'functional brain networks' [5–8]. Such functional networks are usually built by estimating coordination or other interdependencies in the neuronal activity of brain regions.

One can construct functional brain networks using various approaches, such as by measuring blood oxygen level-dependent (BOLD) signals gathered via functional magnetic resonance image (fMRI) scans or by using other modalities [1, 2, 4, 7]. Such studies have yielded many fascinating insights for various disorders and diseases, including Alzheimer's disease [9], autism [10], schizophrenia [11–13] and others [14]. In this article, we examine the effects of two antipsychotics (Aripiprazole and Sulpiride) on the architecture of functional brain networks of both controls (who are deemed to be healthy) and patients who have been diagnosed with schizophrenia.

Schizophrenia is often characterized by abnormal and inconsistent social behaviour, along with failure to differentiate between thoughts and reality. Methods for diagnosing schizophrenia have been somewhat controversial [15], and scientists and doctors seek to understand and develop effective diagnoses and treatment (in the form of therapy and drugs) [16]. Sulpiride, a 'first-generation antipsychotic' (FGA) and hence a 'typical' antipsychotic, works as a selective dopamine agonist and is used for the treatment of schizophrenia [17]. The 'atypical' (and thus 'second-generation antipsychotic' (SGA)) drug Aripiprazole, which acts as a partial dopamine agonist, is also used to treat schizophrenia [18, 19]. FGAs are cost-effective and have been demonstrated to effectively alleviate positive symptoms, but they carry a risk of extrapyramidal effects (including dystonia, parkinsonism and tremor). SGAs have the desirable property of avoiding extrapyramidal effects, but they often come with metabolic side effects and are far more costly. Studies are not conclusive as to which drug type is most effective, and identifying the best course of treatment is a complex issue that varies substantially and must be tailored carefully for each individual [20, 21]. The effectiveness of Sulpiride and Aripiprazole has been reported widely in the literature, and their use for treatment has been approved in many countries [22, 23] (though the United States, Canada and Australia are notable exceptions). The biological mechanisms of Aripiprazole and Sulpiride are well-understood, but their effects at the functional level of the brain are not. This motivates our goal to explore the effects of these drugs on the architecture of functional brain networks.

It has been hypothesized that schizophrenia is related to abnormalities in the connectivity between components of functional brain networks [11]. An important property of a functional brain network—one that appears to be abnormal in patients who are diagnosed with schizophrenia—is community structure [2, 24]. Loosely speaking, a community is a set of nodes in a network that are connected densely to each other but connected sparsely to other parts of a network [25, 26]. Community structure in a network is one type of mesoscale organization, and both community structure and other mesoscale organizations (e.g., core–periphery structure [27]) are important in a variety of contexts in functional brain

networks [2]. Although the effects that antipsychotics have on fMRI data have been examined previously [28], few studies have considered the effects of antipsychotics on functional brain networks [13, 29]. In our exploration of such effects, we focus on community structure of functional brain networks and how it is affected by different antipsychotics.

Our research is based on two working hypotheses. The first one is that community structure is a relevant mesoscale structure that may be informative for diagnosing a particular disease. To examine community structure in individuals who are deemed to be healthy (i.e., 'controls') versus individuals with schizophrenia ('patients') under the effects of different drugs, we employ several characterizations of graph similarity. We consider both basic features (such as the number of common edges) and more sophisticated ones (such as how community structure changes across different scales of a network [30]). This suite of techniques allows us to build a set of distance matrices between subjects, and we apply unsupervised clustering algorithms to these matrices to try to identify discernible groups of subjects. Our second working hypothesis is that the effects of different antipsychotics leave a measurable fingerprint on a network's community structure. To evaluate this hypothesis, we focus on studying the effects of each drug within a given group (intra-subject comparisons), and we also compare groups who have been given the same drug (inter-subject comparisons). We thereby investigate both the difference between controls and patients and the effects that each of the drugs have on the functional brain networks of each group of subjects.

Our article proceeds as follows. In Section 2, we briefly discuss the employed data set and some relevant previous studies, including a contrast with the recent paper [29] in particular. In Section 3, we detail the protocol and the methods that we use to make comparisons between groups of subjects. In Section 4, we present our results. Finally, in Section 5, we discuss the implications of our findings. We include additional details and technical results in a trio of appendices. For example, we give the statement and proof of a theorem (that a certain diagnostic has a metric structure) that we use in the main text in Appendix A, and we discuss an urn-type model to assess the statistical significance of our results in Appendix B.

2. Data and previous studies

We study a data set, which came from Bristol Myers Squibb (BMS) and which we call the 'BMS data set', of measurements of 15 human subjects ('controls') who were deemed to be healthy and 12 human subjects ('patients') who were diagnosed previously with schizophrenia. All participants were pretreated with Domperidone on all three days to reduce side effects. Over three sessions, which were 1–2 weeks apart, each of the 27 subjects was given one of three different drug treatments:

1. ('Placebo') Oral placebo, 180 and 90 min before scanning;
2. ('Sulpiride') Oral placebo, 180 min before scanning; and then oral Sulpiride (400 mg), 90 min before scanning;
3. ('Aripiprazole') Oral Aripiprazole (15 mg), 180 min before scanning; and then oral placebo, 90 min before scanning.

All participants and investigators were blind to the drug condition. All participants were provided with a detailed Patient Information Sheet (PIS) that explained the nature of the pharmacological experiment (comparison of single doses of the two drugs being used for the treatment of schizophrenia with placebo pill) and the double-dummy design.

At each session, after being given one of the drug treatments, each individual was placed in an fMRI scanner to measure blood flow, at resting state, in the brain. The fMRI scanner captures a single image once every 2 s. The scans lasted 17 min and 4 s, so each BOLD time series has 512 time points. The data are parcellated into 298 regions of interest (RoIs), and each region corresponds to a node in a functional brain network. We used an anatomically-driven parcellation scheme and methodology, as described in [31], to partition the data for each subject into 325 contiguous regions, which were as uniform as possible. However, 27 regions did not have high-quality fMRI time series for one or more individuals and were later removed from all subjects, leading to a total of 298 homogeneously-sized regions. Each region has a corresponding time series that represents an average level of activity in that region. We remove four controls (2, 8, 10 and 14) and three patients (3, 5 and 11) from our calculations due to missing data and/or problems due to head motion. We thus examine a total of 20 subjects: 11 controls and 9 patients. (However, we use the original numerical labels for the subjects.) See [32–34] for discussions of issues with head motion, and see [35, 36] for discussions of preprocessing of fMRI data to correct for head motion.

There have been three other studies [11, 29, 37] that employed this particular data set. References [11, 37], which were published a few years ago, focused on the task of distinguishing controls from patients who had been diagnosed with schizophrenia, so they were trying to find effective biomarkers for schizophrenia. Using a parcellation with 90 RoIs, Ref. [11] reported that the patients have 'less strongly connected' brain networks (in the sense of a lower mean pairwise wavelet coherence between regions) and 'more diverse' profiles (in the sense of larger mean variances in a wavelet coherence between a given region and the others) of brain functional connectivity than the controls. They also calculated that brain networks in the schizophrenia group have a greater robustness to uniform-at-random removal of nodes, in the sense that the number of nodes in the largest connected component (LCC) decays more slowly as a function of the number of removed nodes. Reference [37] built functional networks via 'spatial pairwise clustering' (a novel approach that they introduced) of individual voxels (thereby foregoing the need to choose a parcellation) and combining spatially proximate voxels into nodes. In their computations, they observed weaker inter-nodal correlations in patients than in controls. Finally, using a very similar parcellation to the one that we employ but with different techniques from network analysis, a very recent paper [29] studied the effects of the drugs on (1) the networks of the subjects and (2) the subjects' cognitive abilities. Their results suggest that (1) Aripiprazole has a major effect on the networks of controls and that (2) both drugs make it harder to distinguish between controls and patients. This study also found that Aripiprazole diminished the performance of controls at a working-memory task.

3. Methods and preliminary computations

We illustrate our analysis pipeline with a schematic in Fig. 1. In Sections 3.1 and 3.2, we briefly describe how to build a functional network from fMRI time series using wavelet correlations and thresholding techniques (see Step 1 in Fig. 1). In Section 3.3, we discuss our preliminary computations on our collection of networks. In Sections 3.4 and 3.5, we discuss how to define two distance functions to examine dissimilarities of functional networks (see Step 2 in Fig. 1) and how to apply hierarchical clustering to cluster similar subjects (i.e., similar functional networks) according to Step 3 in Fig. 1.

3.1 *Building the networks*

Wavelet-based correlations allow one to examine functional similarities between brain regions based on activity in a specified frequency interval (a so-called wavelet 'scale'). We use the maximal-overlap discrete wavelet transform [38] to decompose each regional mean fMRI time series (see Step 1 in Fig. 1). Examining wavelets is useful for studying resting-state fMRI data, and functional connectivity between

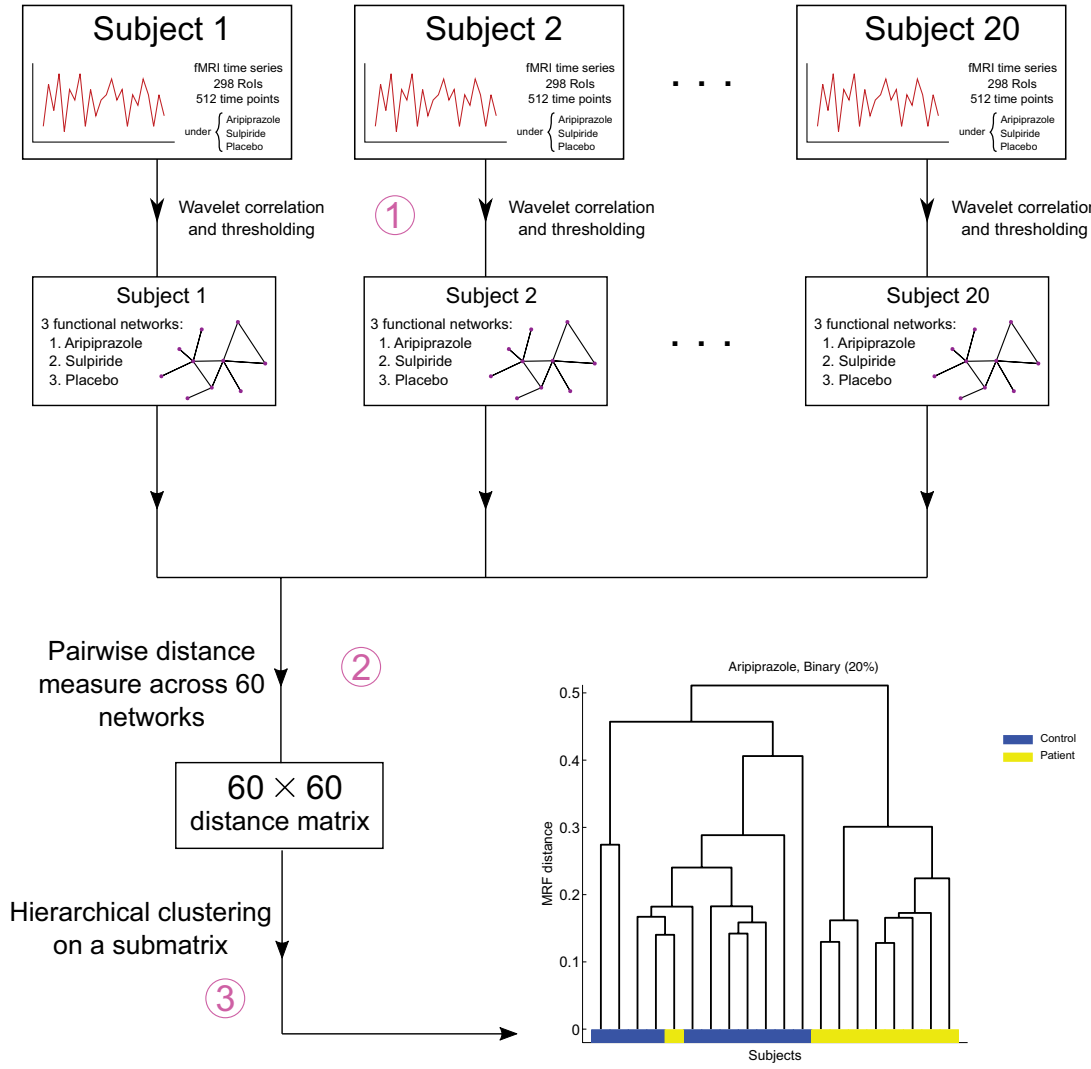

FIG. 1. Protocol to obtain a dendrogram that conveys hierarchical clustering of a set of subjects. There are 20 subjects, and there are three different drug treatments for each subject. This yields 60 networks, and we compute a distance between each pair of networks. This yields a 60×60 distance matrix. (As we discuss in Section 3.4, we construct such a matrix for two different notions of distance.) We do hierarchical clustering using various submatrices of each distance matrix, where the submatrix that we use depends on our particular comparison from Fig. 6. We explain the vertical axis (which uses a particular choice of distance) in the dendrogram in Section 3.4.2. In the example dendrogram in this schematic, we consider unweighted networks that include the strongest 20% of the edges (see Section 3.1).

regions is typically largest at certain frequency bands (below 0.1 Hz) [39]. Let g_i denote the time series of node (i.e., RoI) i (where $i \in \{1, 2, \ldots, 298\}$), and let $V_s(g_i)$ denote the vector of scale-s wavelet coefficients of g_i. At scale s, the connection strength between two nodes, i and j, in a functional network is given by

the wavelet correlation

$$F_{ij} = \frac{\sum_k V_{s,k}(g_i) V_{s,k}(g_j)}{\sqrt{(\sum_k (V_{s,k}(g_i))^2 (\sum_k (V_{s,k}(g_j))^2}} \in [-1, 1]. \quad (1)$$

We compute values of F_{ij} for scales $s = 1, 2, 3, 4$; and we then choose to work with the most informative scale (see Section 4).

There are $N = 298$ RoIs for each subject, so we extract functional networks with $N = 298$ nodes. This yields a similarity matrix $\mathbf{F}$ whose elements are given by Eq. (1). To avoid negative weights,[1] we transform $\mathbf{F}$ into a weighted adjacency matrix $\mathbf{W}$ by taking $W_{ij} := (F_{ij} + 1)/2 \in [0, 1]$. The associated network is fully connected by construction, and there are two customary ways to prune edges. These are (1) thresholding the networks by keeping a fixed fraction τ of the strongest weights (assigning the remaining edges a weight of 0 and producing thresholded weighted networks) and (2) first performing the previous step and then subsequently setting the remaining edges to have a weight of 1, thereby producing thresholded binary networks. In both cases, the resulting thresholded networks have $E \approx N(N-1)\tau/2$ edges. (The reason for the approximation symbol is that we need to round E to an integer.) Of course, one can also simply keep all edges and examine the original fully connected, weighted networks. In this article, we initially examine the original networks and both the weighted and binary thresholded networks. Based on some preliminary calculations, we will then decide which of these networks to examine further.

3.2 *Choosing a scale and thresholding parameter*

To construct the functional networks, we choose a wavelet scale s and then consider thresholding the networks (with an associated threshold value). Previous work has noted differences in both 'connectivity' (i.e., the mean edge weight of a network) and mean local clustering coefficient between controls and patients with schizophrenia [11, 41, 42]. The observed differences were more statistically significant at lower frequencies, and they were particular evident at scale 2. This is consistent with previous research on resting-state fMRI [43]. To make an educated choice of scale, Ref. [11] calculated the mean value of F_{ij} over controls and patients for each scale, performed a t-test, and selected the scale with the smallest p-value. We follow a similar procedure, but we also threshold the networks for both binary and weighted versions using a thresholding parameter τ, such that we keep a fraction τ of the strongest edges (i.e., those with the largest weights).[2] (For example, if $\tau = 0.4$, we keep the strongest 40% of the edges.) For each of the three drug treatments and for each of the scales 1, 2, 3 and 4, we then perform a t-test on the mean local clustering coefficients of controls and patients. In Fig. 2, we show all 12 plots and the p-values associated with the t-tests. Based on these results, we make two decisions. First, from now on, we use scale 2 (which corresponds to the frequency band 0.060–0.125 Hz), because it has the smallest p-values (in agreement with previous work [11]). For very small values of τ, we observe spikes in the p-values that likely arise from the networks breaking up into many components. Second, because our results on binary networks have smaller p-values than the corresponding ones for weighted networks, we focus our

[1] There are also other ways to transform $\mathbf{F}$ into a weighted adjacency matrix $\mathbf{W}$. For example, one can take the absolute value of the similarity values, though it is then impossible to distinguish negative wavelet similarities from positive ones. The weakness of our approach is that we transform initially strongly negative weights into weights that are near 0, and they then tend to be removed if one subsequently prunes a network by keeping only the most strongly weighted edges of $\mathbf{W}$. Recently, Ref. [40] examined the significance of such negative wavelet similarities.

[2] We consider values of τ in increments of 0.01.

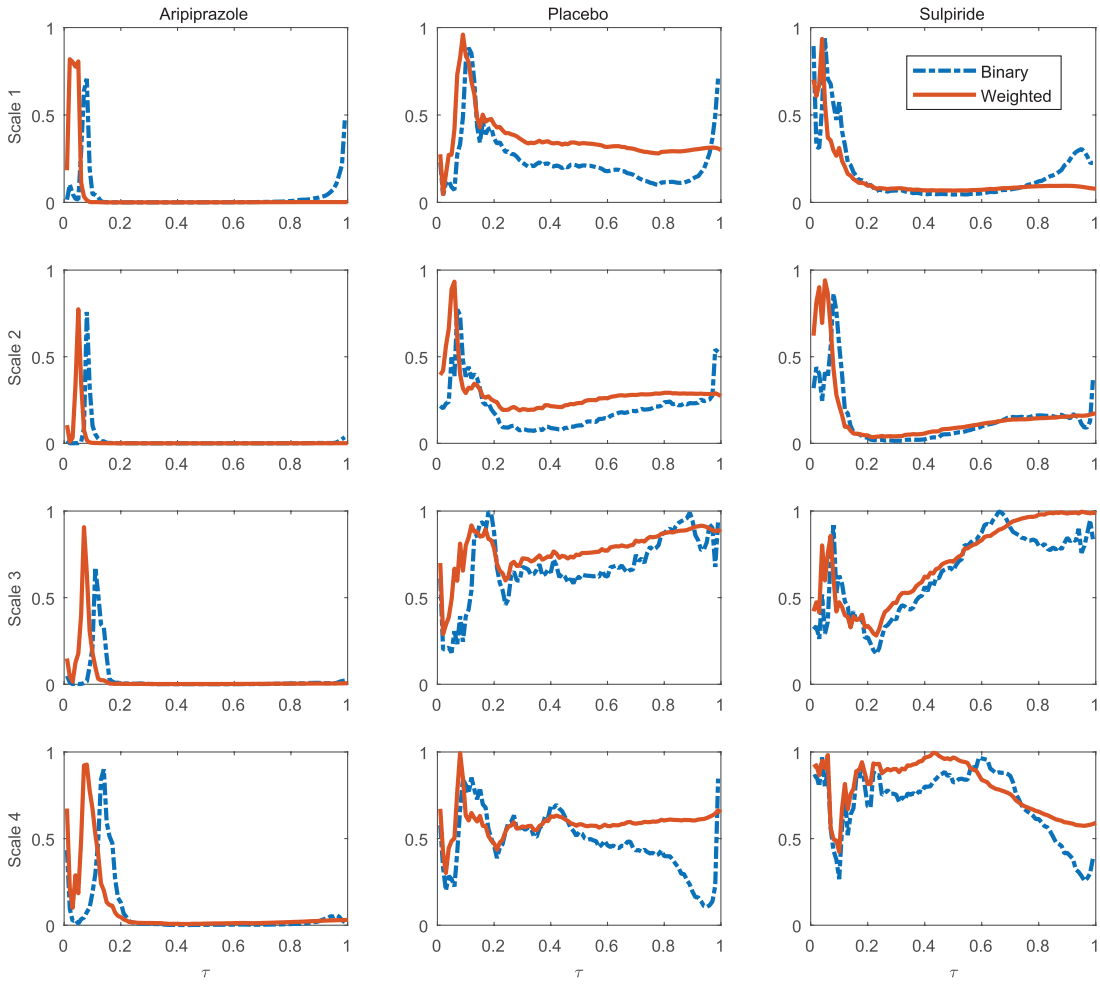

FIG. 2. The p-values associated with t-tests on the mean local clustering coefficient (between patients and controls) for weighted networks (solid orange curves) and binary networks (blue dashed curves) for different values of the thresholding parameter τ. Wavelet scale 2 produces the smallest p-values. We also observe differences in the curves associated with the three drug treatments and that the p-values associated with the binary networks are consistently smaller than those for the weighted ones.

subsequent calculations on thresholded binary networks (except for our calculations of connectivity). The controls tend to have much larger edge weights than the patients, so our comparisons between patients and controls are more directly parallel if we use binary networks, as many network quantities are affected in nontrivial ways by edge weights. From now on, we fix $\tau = 0.2$. (We repeat our calculations for several values of $\tau \in [0.2, 0.4]$, and we obtain qualitatively similar results.)

Half of our networks (30 out of 60) have more than one component when $\tau = 0.2$. This can be problematic for some types of computations, such as those that involve path lengths. In practice, however, this issue did not cause problems in our investigation; the LCC of each network has almost the maximum

of 298 nodes, with the exception of Control 5 on Aripiprazole, whose LCC has 268 nodes. In Appendix C, we show the number and sizes (i.e., numbers of nodes) of the components in each of our networks.

3.3 *Connectivity and mean local clustering coefficient*

We now do some preliminary calculations. Previous research using thresholded, binary networks has highlighted significant differences in 'connectivity' (defined, for an individual subject, as the mean edge weight $\langle W_{ij} \rangle$ of a network) and mean local clustering coefficients of networks from control subjects versus those from patients who were diagnosed with schizophrenia [11]. In our case, by construction, connectivity corresponds (up to a scaling and a shift) to the mean wavelet correlation. For weighted networks, we compute the weighted local clustering coefficient [44]

$$c_i = \frac{1}{k_i(k_i-1)} \sum_{j,k} (W_{ij} W_{ik} W_{jk})^{1/3} \quad \text{for } k_i \geq 2\,, \tag{2}$$

where k_i is the degree of node i and $c_i = 0$ for $k_i \in \{0, 1\}$. Equation (2) reduces to the usual local clustering coefficient for the special case of binary networks.

For connectivity, we calculate $\langle W_{ij} \rangle$ for each subject, and we then calculate the means for both controls and patients. We follow the same process for the local clustering coefficient. In our preliminary analysis, we explore how these basic quantities differ for different drug treatments. Specifically, we calculate connectivity using the non-thresholded weighted versions of the networks and mean local clustering coefficient using the thresholded binary networks. We show our results in Fig. 3, where for each case we plot the mean and standard deviation across subjects. For each drug treatment, we also perform a two-sample t-test on the values of connectivity and mean local clustering coefficients for controls and patients, and we extract a p-value. We observe small differences in connectivity and mean local clustering coefficients between controls and patients; this difference is smaller than what was reported previously with these data using other approaches [11]. We also observe that Aripiprazole has a small effect on the connectivity and mean local clustering coefficients of controls but no significant effect on patients, in agreement with other recent work [29]. Sulpiride appears to have little effect on either group, though we observe a larger difference between controls and patients for mean local clustering coefficient than we do for connectivity. We obtain a p-value of $p \approx 0.0326$ for mean local clustering coefficient and a p-value of $p \approx 0.1680$ for connectivity. We show the connectivity for all subjects under placebo in Fig. 4, and we note that Patient 8 has a very large value of connectivity. However, given the sizes of the error bars, we cannot reject the hypotheses that the connectivity and/or mean local clustering coefficients are indistinguishable in the different situations. This suggests either that (1) this data set is not large enough for these measures to detect robust differences and/or that (2) these simple network diagnostics may not give clear information about whether the drugs have any discernible effects on the architecture of functional brain networks. Given the inconclusiveness of these results, we need to do a more sophisticated analysis.

3.4 *Distance measures*

As we mentioned in Section 1, we aim to classify similar functional brain networks using unsupervised clustering of subjects. A subject is associated with a functional network. To classify these networks in a systematic way, we define a pairwise distance function between graphs, and we then use this function

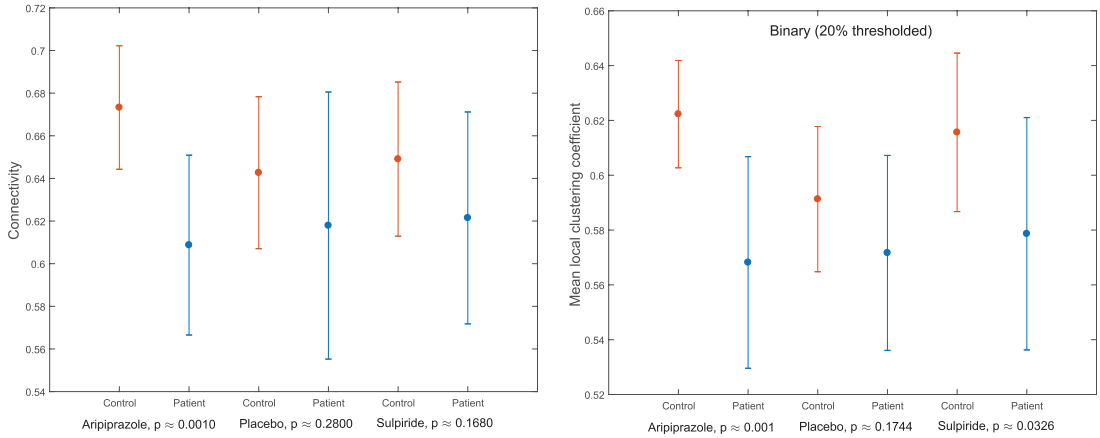

FIG. 3. Means and standard deviations of (left) connectivity for non-thresholded weighted networks and (right) mean local clustering coefficients for binary networks thresholded to 20% of the strongest edges. The results are similar in each case, though we observe for Sulpiride that the controls and patients have different p-values for the two-sample t-test.

to compute a distance matrix for a set of subjects. (See Step 2 in Fig. 1.) We consider distance functions based on two rather different aspects of networks.

3.4.1 *Hadamard-like distance.* One can construct a simple similarity measure between binary networks **A** and **B** that both have the same number of edges by computing the Hadamard product of the matrices and then summing the entries $A_{ij}B_{ij}$ of the resulting matrix. For binary networks, this sum ($\sum_{i>j} A_{ij}B_{ij}$) is the number of common edges in the networks. (We sum over $i > j$ because our networks are undirected.) Because it is common to threshold functional networks so that one retains only a specified, fixed fraction of edges, we can use this similarity measure to compare adjacency matrices that we extract from thresholded functional networks. We define the metric

$$d_1(\mathbf{A}, \mathbf{B}) = 1 - \frac{1}{E} \sum_{i>j} A_{ij}B_{ij} \in [0, 1], \tag{3}$$

which is well-defined when **A** and **B** have the same number E of edges.

We have proven rigorously (see Appendix A for the precise statement of the theorem and its proof) that d_1 satisfies the properties of a metric. We can then construct a distance matrix $\mathbf{D}^1$, whose element $\mathbf{D}^1_{\alpha\beta}$ gives the distance between the functional networks of subjects α and β. Using $\mathbf{D}^1$ has the advantage of being computationally efficient and based on a mathematically sound metric, although d_1 is a rather simplistic measure—two networks are more distant from each other when they have fewer common edges—and we do not expect it to capture certain details (e.g., community structure) of the networks.

3.4.2 *Distance based on community structure.* We also use a more sophisticated distance measure, introduced by Onnela *et al.* [30], that is based on network community structure [25, 26]. It requires using a method of partitioning that assigns each node to a community (i.e., it is a 'hard partition'). In this article, we use modularity maximization [45, 46] and employ the code of Onnela *et al.* that implements the (locally greedy) Louvain method [47].

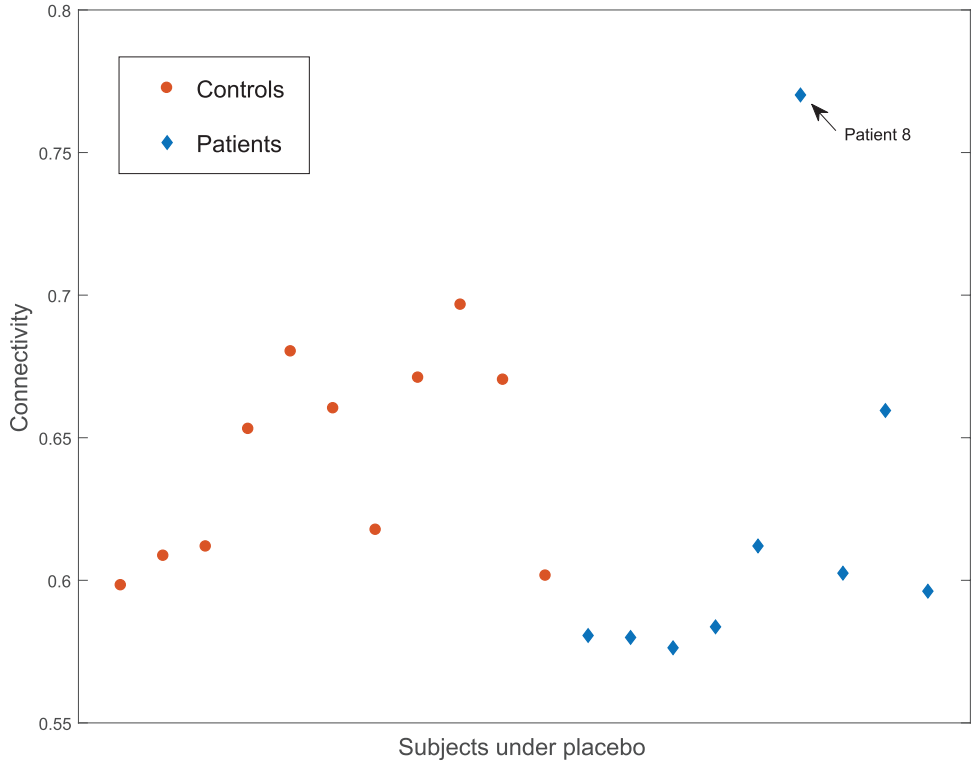

FIG. 4. Connectivity of each subject under placebo. We observe that Patient 8 has an abnormally large value of connectivity. (Recall that we removed Patients 3 and 5 from consideration because of missing data and problems with head motion, but we use the original numerical labelling of the subjects.)

Given a network described by its weight matrix $\mathbf{W}$, one can detect communities in it by maximizing modularity, which one does by minimizing the objective function

$$\mathcal{H}(\gamma) = -\sum_{i \neq j} \left(W_{ij} - \gamma \frac{r_i r_j}{2M} \right) \delta(C_i, C_j), \tag{4}$$

where γ is a resolution parameter, C_i is the community assignment of node i (and C_j is the community assignment of node j), r_i is the strength (i.e., sum of incident edge weights) of node i, and M is the total edge weight. We consider undirected networks, so we use the Newman–Girvan null-model matrix $\mathbf{P}$ with elements $P_{ij} = r_i r_j/(2M)$ [46, 48]. The quantity $W_{ij} - P_{ij}$ is the 'effective weight' of the edge between nodes i and j. For unweighted networks, node strength reduces to degree (i.e., $r_i = k_i$ and $r_j = k_j$), and the total edge weight reduces to the total number of edges (i.e., $M = E$). For each value γ, minimizing the objective function (4) gives a partition of a network into disjoint communities. The quantity $\mathcal{H}(\gamma)$ also quantifies the (scaled) energy of the system [49]. For illustration, we show a particular partition of a functional brain network into communities in the left panel of Fig. 5. (See the middle panel of the same figure for the same network embedded in a three-dimensional (3D) physical space, where node locations correspond to the actual physical regions.)

Onnela *et al*. defined 'mesoscopic response functions' (MRFs) for three quantities that describe, from different perspectives, how a partition of a network changes as a function of γ. In calculating a network's MRF, one varies the parameter γ between $\gamma_{\min}$ (where community detection yields a single community) and $\gamma_{\max}$ (where each node is assigned to its own community). Let n_k denote the number of nodes in community k and define $p_k = n_k/N$ to be the probability of choosing a node uniformly at random from community k. One can then define a partition entropy of the associated community-size distribution as $\mathcal{S}(\gamma) = -\sum_{k=1}^{\eta(\gamma)} p_k \log(p_k)$, where $\eta(\gamma)$ is the number of communities. One then defines the effective energy ($\mathcal{H}_{\text{eff}}$), effective entropy ($\mathcal{S}_{\text{eff}}$) and the effective number of communities (η_{eff}) as follows:

$$\mathcal{H}_{\text{eff}}(\gamma) = \frac{\mathcal{H}(\gamma) - \mathcal{H}(\gamma_{\min})}{\mathcal{H}(\gamma_{\max}) - \mathcal{H}(\gamma_{\min})} = 1 - \frac{\mathcal{H}(\gamma)}{\mathcal{H}(\gamma_{\min})}\,, \tag{5}$$

$$\mathcal{S}_{\text{eff}}(\gamma) = \frac{\mathcal{S}(\gamma) - \mathcal{S}(\gamma_{\min})}{\mathcal{S}(\gamma_{\max}) - \mathcal{S}(\gamma_{\min})} = \frac{\mathcal{S}(\gamma)}{\log(N)}\,, \tag{6}$$

$$\eta_{\text{eff}}(\gamma) = \frac{\eta(\gamma) - \eta(\gamma_{\min})}{\eta(\gamma_{\max}) - \eta(\gamma_{\min})} = \frac{\eta(\gamma) - 1}{N - 1}\,. \tag{7}$$

One uses a parameter ξ that tracks, in a discrete manner (keeping track of when each effective weight changes sign), which edges have a positive effective weight and which have a negative effective weight. By construction, varying γ from $\gamma_{\min}$ to $\gamma_{\max}$ corresponds to varying ξ from 0 to 1. For a detailed discussion, see [30].

To each network, one associates a curve for each of $\mathcal{H}_{\text{eff}}$, $\mathcal{S}_{\text{eff}}$ and η_{eff} (or for any other quantity that one wishes to track [50]) as a function of ξ; these are the MRFs. In the right panel of Fig. 5, we show example MRFs that we compute from our functional brain networks. We show average MRFs (which we compute as a pointwise mean of the MRFs for the 60 networks), along with the maximum and minimum MRFs (which we determine based on ordering the area under the curve of each MRF from largest to smallest), of these networks.

To compare a pair of networks, we compare the differences in their profiles. Consider a pair of networks, α and β, along with the following three distances:

$$d^{\mathcal{H}}_{\alpha\beta} = \int_0^1 \left| \mathcal{H}^{\alpha}_{\text{eff}}(\xi) - \mathcal{H}^{\beta}_{\text{eff}}(\xi) \right| d\xi\,, \tag{8}$$

$$d^{\mathcal{S}}_{\alpha\beta} = \int_0^1 \left| \mathcal{S}^{\alpha}_{\text{eff}}(\xi) - \mathcal{S}^{\beta}_{\text{eff}}(\xi) \right| d\xi\,, \tag{9}$$

$$d^{\eta}_{\alpha\beta} = \int_0^1 \left| \eta^{\alpha}_{\text{eff}}(\xi) - \eta^{\beta}_{\text{eff}}(\xi) \right| d\xi\,. \tag{10}$$

The three distances in Eqs. (8)–(10) capture different aspects of community structure. The effective energy ($\mathcal{H}_{\text{eff}}$) is a rescaled version of the objective function $\mathcal{H}$, the effective entropy ($\mathcal{S}_{\text{eff}}$) quantifies the amount of heterogeneity in the sizes of the detected communities, and the effective number of communities (η_{eff}) is a rescaled version (with respect to network size) of the total number of communities. From these distances matrices, we construct a single distance matrix by projecting each 3D coordinate using principal

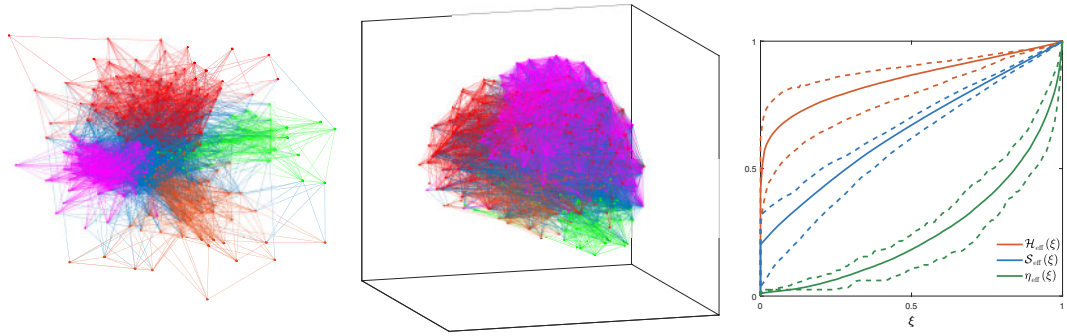

FIG. 5. An example, which we show both (left) in 2D and (right) in 3D, of a particular network (Control 1 on placebo) partitioned into communities for a specific value of the resolution parameter ($\gamma = 1$, so $\xi \approx 0.02$). (Right) An average MRF, which we determine by taking a pointwise mean of the MRFs of all 60 networks, along with the maximum and minimum curves (based on the area under each MRF curve). For each colour, the upper curve is the maximum, the middle curve is the pointwise mean, and the bottom curve is the minimum. We show $\mathcal{H}_{\text{eff}}(\xi)$, as defined in Eq. (5), in orange; we show $\mathcal{S}_{\text{eff}}(\xi)$, as defined in Eq. (6), in blue; and we show $\eta_{\text{eff}}(\xi)$, as defined in Eq. (7), in green.

component analysis (PCA) and keeping the first component. That is, we construct a distance matrix by calculating a linear combination of the three distance measures:

$$d^P_{\alpha\beta} = w_{\mathcal{H}} d^{\mathcal{H}}_{\alpha\beta} + w_{\mathcal{S}} d^{\mathcal{S}}_{\alpha\beta} + w_{\eta} d^{\eta}_{\alpha\beta} \,, \tag{11}$$

where the weights w_ℓ (with $\ell \in \{\mathcal{H}, \mathcal{S}, \eta\}$) are the coefficients of the first principal component. There are a total of 60 networks (11 controls and 9 patients, each of which is on three different drug treatments). We calculate a matrix with $60 \times 59/2$ (the total number of network pairs) rows and 3 columns, where each column corresponds to the vector representation[3] of the upper triangle of one of the distance matrices $\mathbf{D}^{\mathcal{H}}$, $\mathbf{D}^{S}$ and $\mathbf{D}^{\eta}$. We perform a PCA on this matrix to create a distance matrix $\mathbf{D}^{P}$.

The final outcome of the above calculation is a 60×60 distance matrix $\mathbf{D}^{P}$, where each entry measures the distance between networks α and β based on how the community structure of each network varies as a function of the parameter ξ. We henceforth use the term 'MRF distance' for the quantity that we compute in Eq. (11).

3.5 *Hierarchical clustering*

Once we have our distance matrix (see Section 3.4.2), we take a submatrix of it for each of the comparisons in Fig. 6. For example, if we are comparing controls and patients under the drug Aripiprazole, we keep only the rows and columns that correspond to this drug, leaving us with a 20×20 distance matrix, where the rows and columns correspond to the 11 controls and 9 patients. We then cluster the new, smaller distance matrix using one of numerous possible methods. For simplicity, we use average linkage clustering to group similar subjects (i.e., similar networks) together and show our results in the form of dendrograms. We then order the leaves of the dendrogram to maximize the sum of the similarities between adjacent leaves by reordering its branches (without further partitioning of the clusters). We colour the leaves of

[3] We obtain a vector via concatenation, which we do row by row using the 'squareform' command in MATLAB.

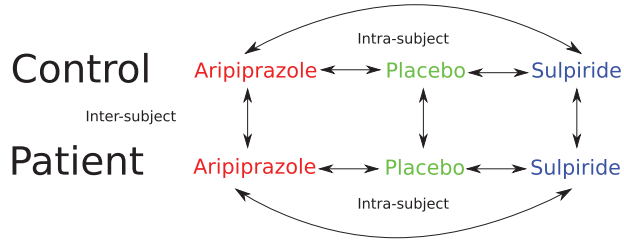

FIG. 6. Illustration of possible comparisons between the groups of subjects and different drug treatments.

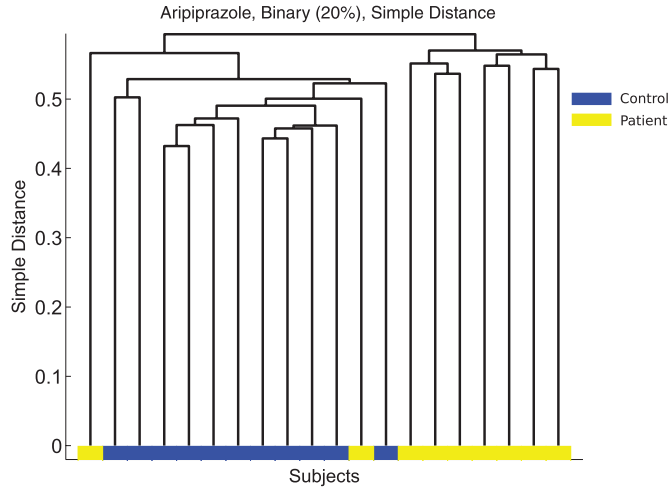

FIG. 7. Dendrogram for the drug Aripiprazole in which we compare the 11 controls and 9 patients using the distance measure $d_1(\mathbf{A}, \mathbf{B})$. There is some separation between patients and controls.

the dendrograms based on their annotations: patients or controls without drugs, patients or controls on one drug, or patients and controls on the other drug.

4. Main results

As we mentioned in Section 1 and depicted in Fig. 6, we make a total of nine comparisons, including both inter-subject ones (different groups under the effect of the same drug) and intra-subject ones (the same group under the effect of different drugs). In our ensuing discussions, we present the results of these comparisons.

4.1 *Inter-subject comparisons*

We do inter-subject comparisons using the procedure that we outlined in Fig. 1. We start by comparing controls and patients under the effects of the drug Aripiprazole using the simple distance measure $d_1(\mathbf{A}, \mathbf{B})$ from Eq. (3). We show the resulting dendrogram in Fig. 7. We observe some separation between patients and controls.

To do a more sophisticated analysis, we compute a dendrogram from the same data using the MRF distance matrix $\mathbf{D}^P$ (see Section 3.4). We show the resulting dendrogram in Fig. 8. The separation between patients and controls is now better, and we correctly classify almost every individual. The only exception is Patient 8, who is assigned to the same group as the controls. Although this misclassification seems surprising at first, it agrees with our previous calculations (see Fig. 4), which also suggest that Patient 8 has different network characteristics than the other patients.

The above result suggests that, under the drug Aripiprazole, we are able to almost completely distinguish patients from controls, based only on information about their community structure. This also suggests that the distance matrix $\mathbf{D}^P$ incorporates more meaningful information than the simplistic distance measure in Eq. (3), so we use only the former for our subsequent computations.

We show our results from comparing controls and patients under placebo in the left panel of Fig. 9. In this case, we still observe a relatively good separation between patients and controls, in agreement with previous results that functional brain networks encode biomarkers that separate patients diagnosed with schizophrenia from controls [11, 37]. In this situation as well, Patient 8 appears to be more similar to the controls than to the other patients. Even more interesting, we observe a less-clear separation between the controls and patients than we did under Aripiprazole. We thus conclude that Aripiprazole alters community structure for at least one group and that this alteration makes it easier to distinguish between the patient and control groups. However, it is not yet obvious whether Aripiprazole is affecting the architecture of the functional brain networks of patients, controls or both.

In the right panel of Fig. 9, we show our results for computations of functional brain networks for individuals under the influence of Sulpiride. The control and patient groups are now less distinct from each other than they were with placebo. This suggests that Sulpiride has a mild but detectable effect of increasing the similarity between community structures of patients and controls. Again, it is not clear whether Sulpiride affects the functional brain networks of patients, controls or both.

4.2 *Intra-subject comparisons*

To examine the effects of the drug treatments on network architecture, we make intra-subject comparisons, such as comparing the control group under Aripiprazole to the control group under Sulpiride. We do these comparisons using the procedure that we outlined in Fig. 1.

4.2.1 *Aripiprazole versus placebo.* For our intra-subject comparisons (see Fig. 6), we first compare the effects of Aripiprazole on the functional brain networks of controls to those of patients. To do this, we use all 11 controls under Aripiprazole and the same 11 controls under placebo and do average linkage clustering on the associated 22×22 distance matrix with MRF distances. We also do average linkage clustering using the MRF distance for the 18×18 distance matrix that we obtain by considering the nine patients under Aripiprazole and the same patients under placebo.

In Fig. 10, we show the dendrogram for our comparison between Aripiprazole and placebo for patients. At the coarsest level of detail (i.e., a separation for a large MRF distance in the dendrogram), we observe that both the Aripiprazole and placebo network of Patient 8 is grouped away from those of the other patients. This is consistent with our prior results: we saw in Fig. 4 that Patient 8 has a much larger value of connectivity than the other patients and saw in Fig. 8 that Patient 8 was grouped with the controls. At the finest level of detail, we also find for both Aripiprazole and placebo that Patients 4 and 9 cluster close to each other. We thus expect, given the inter-subject comparisons in Section 4.1, that Aripiprazole does affect community structure in controls. We confirm this hypothesis in Fig. 11, where we observe that controls under Aripiprazole are clearly separated from controls under placebo.

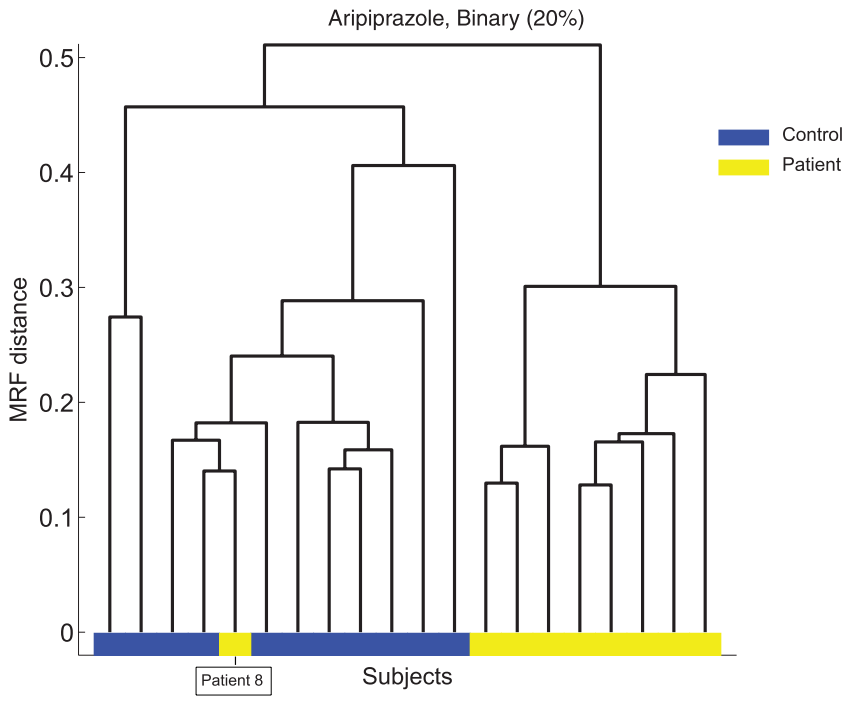

FIG. 8. Dendrogram for our MRF analysis of functional brain networks for the drug Aripiprazole. We compare the 11 controls and 9 patients using the distance measure $\mathbf{D}^P$. There is a clear separation between patients and controls, although Patient 8 appears with the control group.

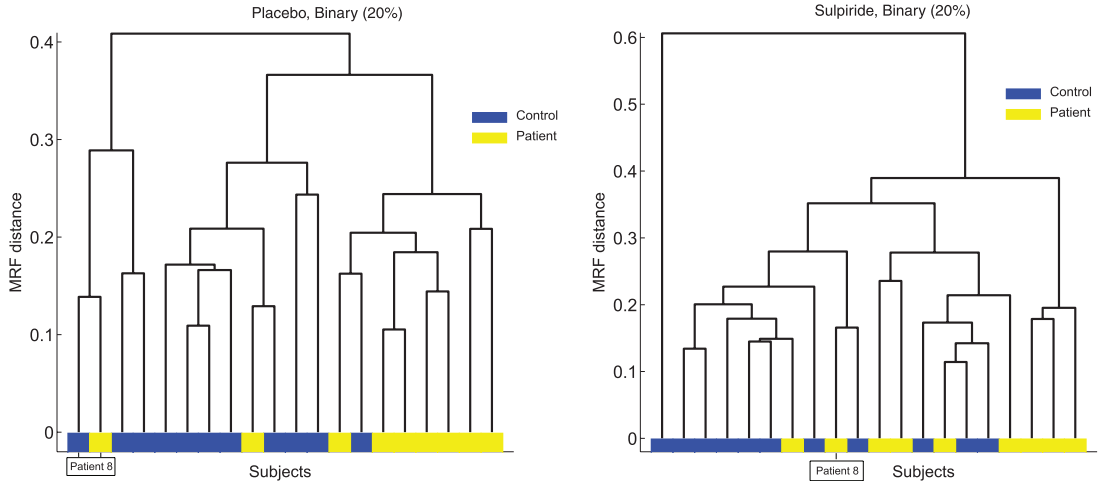

FIG. 9. Dendrogram for our MRF analysis of functional brain networks for (left) placebo and (right) the drug Sulpiride. In order of most successful to least successful (compare this figure to Fig. 8), the clustering performs best for Aripiprazole, second-best for placebo and worst for Sulpiride. (See Section 4.3 for a quantitative justification of this observation.)

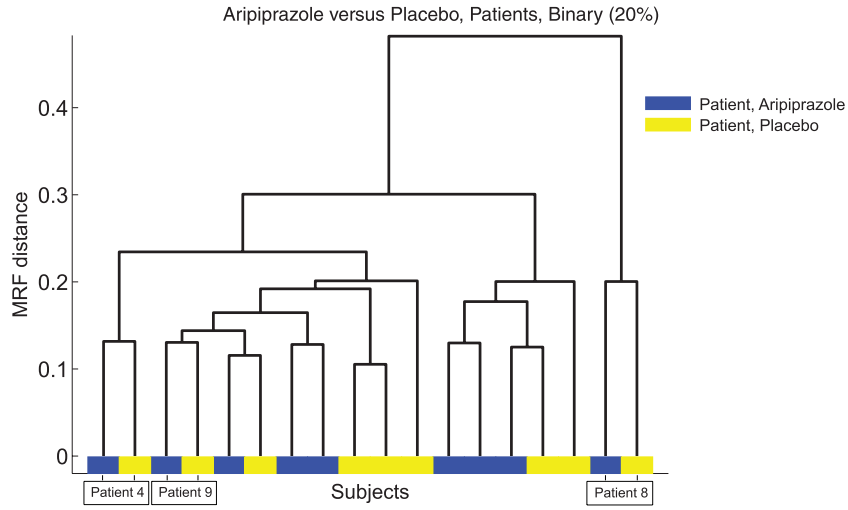

FIG. 10. Dendrogram for our MRF analysis of functional brain networks for our comparison between Aripiprazole and placebo for the patient group. Each patient thus appears twice on the horizontal axis. There is no clear separation between the two drugs, and the two instances of some patients (e.g., 4, 8 and 9) cluster very close to each other, suggesting that there is very little difference in community structure in the networks under placebo and under Aripiprazole in these patients.

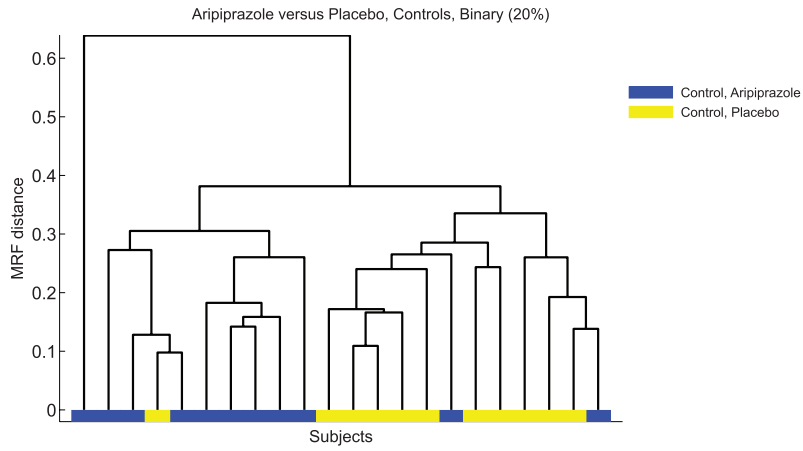

FIG. 11. Dendrogram for our MRF analysis of functional brain networks for our comparison between Aripiprazole and placebo for the control group. We observe a mostly clear separation between networks under the two drug treatments.

4.2.2 *Sulpiride versus placebo.* In Section 4.2.1, we observed a very clear separation between controls and patients under the drug Aripiprazole, and we also observed evidence (though the situation is less clear) of separation under placebo. We observed less separation between controls and patients under Sulpiride. We hypothesized that Sulpiride has a mild but detectable effect of increasing the similarity between community structure in patients and controls, and we therefore suggest that Sulpiride affects community structure in either patients or controls (or both), in agreement with [29]. In Fig. 12, we show

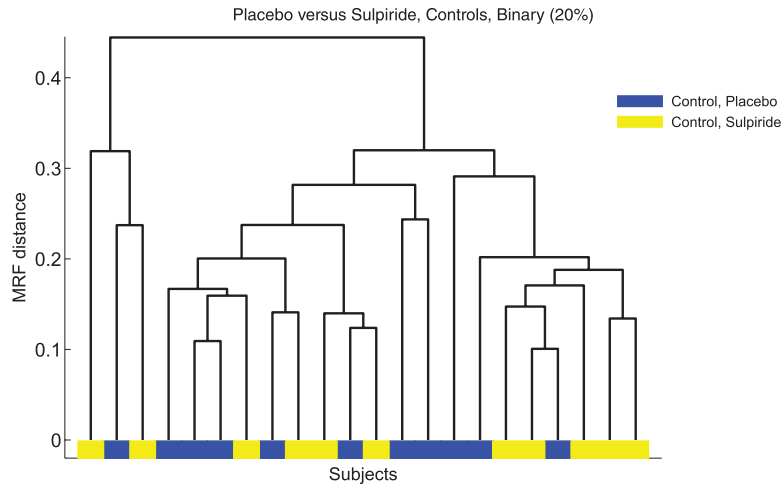

FIG. 12. Dendrogram for our MRF analysis of functional brain networks for our comparison between Sulpiride and placebo for the control group.

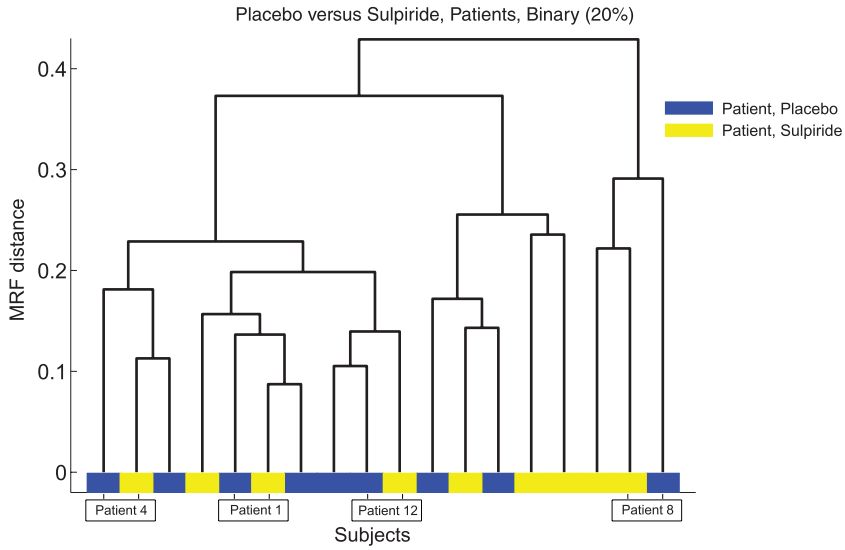

FIG. 13. Dendrogram for our MRF analysis of functional brain networks for our comparison between Sulpiride and placebo for the patient group. As with our comparison of placebo to Aripiprazole, several identical patients appear close together and Patient 8 is again distant from the others.

a dendrogram of the intra-subject comparison of placebo versus Sulpiride in controls. We do not observe any clear clustering, and we also do not observe clear clustering in the same comparison for patients (see Fig. 13). Therefore, we do not find any clear indication of why Sulpiride seems to make controls and patients less distinguishable from each other. Additionally, we do not observe a clear separation under placebo or under Sulpiride either for controls (see Fig. 12) or for patients (see Fig. 13).

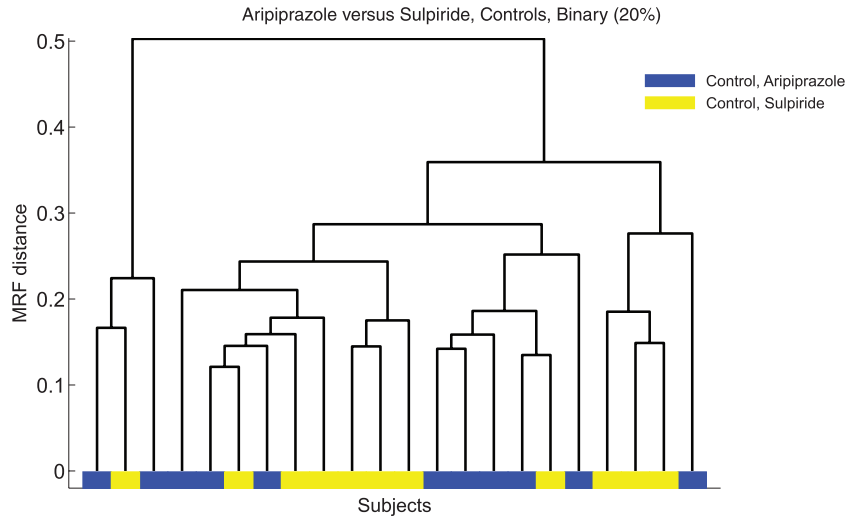

FIG. 14. Dendrogram for our MRF analysis of functional brain networks for our comparison between Aripiprazole and Sulpiride for the control group.

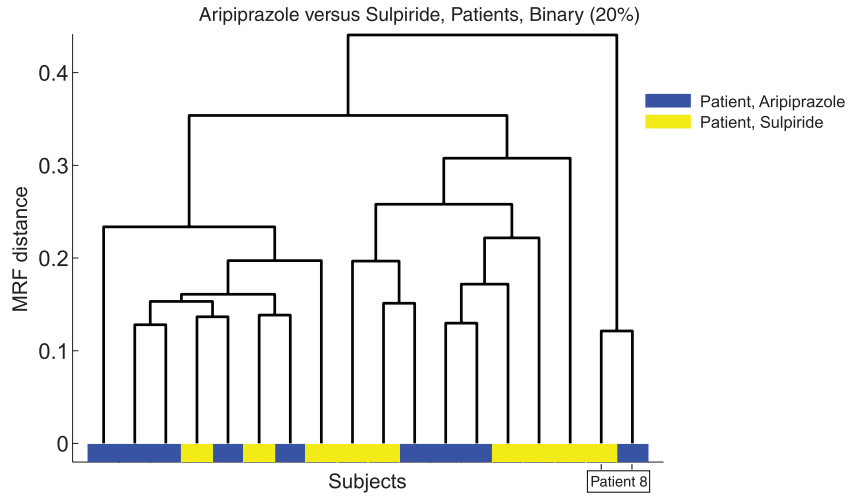

FIG. 15. Dendrogram for our MRF analysis of functional brain networks for our comparison between Aripiprazole and Sulpiride. In both the Aripiprazole and Sulpiride networks, it is once again easy to distinguish Patient 8 from the other patients.

4.2.3 *Aripiprazole versus Sulpiride.* We can partly distinguish controls under Aripiprazole from those under Sulpiride (see Fig. 14). This is unsurprising, given that we found (see Section 4.2.1) that Aripiprazole alters community structure in controls. We do not observe any obvious difference between patients under Aripiprazole and those under Sulpiride (see Fig. 15).

4.3 *Synthesis of our results from hierarchical clustering and quantitative assessment*

Our results from average linkage clustering of collections of functional brain networks using the distance functions yield the following conclusions:

- Aripiprazole affects the community structure of functional brain networks in controls, but not in patients; and it thereby facilitates the distinction between controls and patients under the effect of this drug treatment.
- Sulpiride reduces the distinguishability between patients and controls, although our intra-subject computations were inconclusive in both patients and controls.

4.3.1 *Preliminary quantitative assessment based on purity.* In this article, we used hierarchical clustering as a simple method to observe how individuals cluster. The main reason for choosing this approach over other possibilities (such as k-means clustering) is that dendrograms provide more information about how individuals group at different distances. For instance, we observed in the dendrogram in Fig. 10 that Patient 8 is a clear outlier. If we had instead performed k-means clustering with $k = 2$, we would be left with Patient 8 in one community and the other patients in the other community. It would still seem that Patient 8 is an outlier, but the extent to which this is the case would be obscured. Furthermore, hierarchical clustering gives insights at different scales; for example, in Fig. 10, we observed that, at a finer scale, Patient 4 on Aripiprazole is grouped with Patient 4 on placebo. At a larger scale, we cannot distinguish between patients under Aripiprazole and those under placebo, which itself is an interesting observation.

The above discussion notwithstanding, it is convenient to attach a number to each partition to quantitatively compare different dendrograms, which is potentially desirable to more precisely evaluate our observations, such as the extent to which Aripiprazole is better than Sulpiride at separating controls from patients. We leave a detailed analysis for future work, but we perform a preliminary quantitative justification based on the notion of *purity* [51]. Consider a partition of a set of B binary data points (i.e., each data point, which for us is a node, belongs to one of two classes) into k communities. To compute purity, we assign each community to the more-common class in that community; and we measure the accuracy of this assignment by counting the number of correctly-assigned nodes and dividing by B.

To measure the purity of a dendrogram, we use the following simple recipe. For clustering to emerge in a dendrogram, purity should be a non-monotonic function as a function of the cut level; and we expect it to reach its maximum for a cut at which the number of communities is small (i.e., when the cut is near the top of the dendrogram). More specifically, in a well-clustered dendrogram, we expect that a purity function may peak for a cut with a relatively small number of communities, then stay roughly constant or decay, and finally increase at the bottom of the dendrogram (as, by definition, purity is trivially maximized when each of the communities has just one element). For well-clustered dendrograms, we take the clustering quality as the earliest peak value of the purity function. However, if purity increases monotonically as a function of the number of communities, we conclude that no good clustering emerges in a dendrogram. We sketch three typical shapes (which constitute the three simplest nontrivial possibilities) of the purity function in Fig. 16.

Consider three dendrograms from our inter-subject comparisons: controls versus patients under Aripiprazole (denoted by A; see Fig. 8), controls versus patients under placebo (denoted by P; see the left panel of Fig. 9), and controls versus patients under Sulpiride (denoted by S; see the right panel of Fig. 9). For Sulpiride (S), a dendogram's purity function increases monotonically, so we conclude that there is no good clustering. In other words, one cannot easily distinguish controls from patients under Sulpiride, in agreement with our earlier qualitative results. For both Aripiprazole and Sulpiride, however,

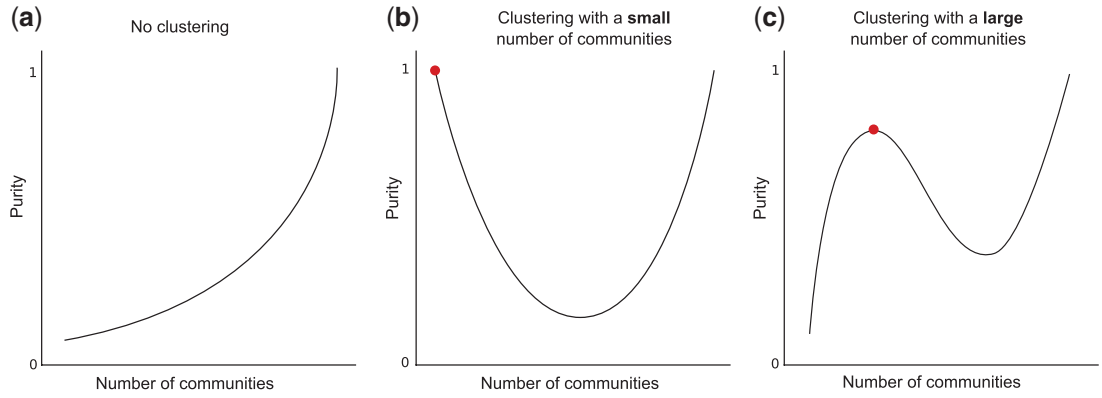

FIG. 16. Three cartoons that illustrate idealized purity curves as a function of the number of disjoint communities in a dendrogram. In (a), purity increases monotonically as a function of the number of communities, so we conclude that no good clustering emerges. In (b), purity decreases to a local minimum, and it then increases towards the trivial maximum as the number of communities approaches the total number of nodes. We highlight the clustering quality with a red dot. (We report the purity value at this location as the quality.) In (c), purity increases to a local maximum, then decreases to a minimum, and finally approaches the trivial maximum. We again highlight the clustering quality with a red dot.

the dendrogram's purity function is not monotonic, so quantifiable clustering emerges. It peaks at $k = 2$ communities for Aripiprazole (A) and at $k = 3$ communities for placebo (P). The values of purity are

$$\text{purity}(\mathsf{A}) = 19/20 \qquad \text{and} \qquad \text{purity}(\mathsf{P}) = 17/20\,,$$

so observable clustering exists in these two cases, but it is stronger under Aripiprazole than under placebo. This also agrees with our prior qualitative results.

4.3.2 *An urn-type null model to assess statistical significance.* Although our preliminary analysis suggests that there are different levels of clustering in the data, because the data set is small (there are only 20 subjects), one cannot rule out the possibility that putative clustering may be contaminated by statistical artefacts or finite-size effects. A simple way to assess 'how probable' it is that the observed amount of clustering arises from chance is to construct an urn-type null model. Our construction and results (see Appendix B for details) suggests that the observed differences are genuine ones, rather than arising simply by chance.

5. Conclusions and discussion

We used network analysis to examine the effects of two antipsychotics—Aripiprazole and Sulpiride—on the architecture of functional brain networks of both controls (who were deemed to be healthy) and patients who were diagnosed with schizophrenia. Our motivation for our study was two-fold: (1) to evaluate whether mesoscale network properties (such as community structure) can distinguish controls from patients who were diagnosed with schizophrenia and (2) to examine how the results of such calculations differ across different types of antipsychotic treatments. Using MRFs, we compared community structures of functional brain networks of both patients and controls under the effects of Aripiprazole, Sulpiride and a placebo.

We will now summarize the results of our computations. However, before doing so, we stress that when interpreting the results of fMRI studies, it is very important to consider the cautionary notes

in [52], who noted that computations with fMRI data (even before constructing any networks from such data) rely on a variety of statistical assumptions of questionable validity. These important complications notwithstanding, our computations produced several interesting results. First, we did a reasonable job of distinguishing between controls and patients under placebo. This result suggests that community structure in functional brain networks is a relevant way to help with diagnoses of schizophrenia. Second, we found that community detection did a much better job (yielding a high-quality clustering) of distinguishing the two groups when Aripiprazole had been administered than for Sulpiride or placebo, suggesting that Aripiprazole has a larger effect on community structure than Sulpiride in at least one of the control group or the patient group. By comparing controls under Aripiprazole and under placebo, we concluded that Aripiprazole appears to improve the distinguishability between patients and controls through its effects on community structure in the control group, rather than in the patient group.

We obtained mixed results for community detection on networks associated with individuals who were treated with the drug Sulpiride. We found that patients who were treated with Sulpiride are closer to controls than they are under either Aripiprazole or a placebo (where no clustering seems to emerge, as discussed Section 4.3). This is also consistent with [29]; and it suggests that Sulpiride has a mild effect on community structure that is appreciably larger than, for instance, the effect of Aripiprazole on community structure in patients (which we observed to be very small). We have not been able to clearly establish the origin of this observation, as our intra-group comparisons suggest that community structure in both controls and patients is mostly unaltered by Sulpiride.

One of the main objectives of an antipsychotic is to manage and reduce symptoms that an individual experiences. For schizophrenia, this involves modifying behaviour and symptoms to cause an individual be more similar, in terms of behaviour and symptoms (or lack thereof), to an average healthy person without the disease. A tempting, but naive, reasoning may suggest that one may therefore expect their associated functional brain networks to also be more similar. This link is poorly understood (though see [29]). Mesoscale network properties, such as communities, are well-known to be important for functional brain networks [2]; and network analysis in general is often useful for disentangling structure, function and their complex interrelations in the brain. However, the link between drug effectiveness and the effect on functional brain networks is not clear; and it both merits and requires further investigation. It is noteworthy that our observations that Aripiprazole primarily affects community structure in controls, rather than patients, is consistent with the results of Towlson *et al.* [29], who reported that Aripiprazole has a radical effect on the organization of the brain networks of controls but decreases the performance of the controls at cognitive tasks. Our work also leaves additional open questions for future work. For instance, an interesting technical point that is worth exploring in more detail is to examine clustering methods other than hierarchical clustering. The sample size (20 subjects) in the experimental data that we studied is small; and conducting new, large-scale experiments is highly desirable to test the validity of our results (although evidence in Section 4.3 and Appendix B suggests that our results are statistically significant).

From a network-science viewpoint, we highlight that we used community structure and MRFs for a classification task in time-independent, monolayer functional brain networks. Extending these results and analysis to time-dependent and multilayer settings [53, 54] is another interesting open problem.

Acknowledgements

LL acknowledges funding from EPSRC Early Career Fellowship (EP/P01660X/1), and RF acknowledges funding from the EPSRC (through DTP EP/N013492/1). SHL was supported by the National Research Foundation of Korea (NRF) through grant number NRF-2018R1C1B5083863. EKT was supported by an EPSRC doctoral studentship. We thank Sebastian Ahnert for helpful discussions, Ameera Patel for

discussions about preprocessing the raw fMRI data, Ulrich Müller for recruiting and scanning participants in the original experimental work, and Melissa Lever for early computational work on this project. Data collection was supported by a grant from Bristol Myers Squibb to Robert Kerwin at King's College London. There is formal NHS ethics-committee approval to perform the study, but we are not able to acquire similar approval to release the anonymized data.

References

1. Bassett, D. S. & Sporns, O. (2017) Network neuroscience. *Nat. Neurosci.*, **20**, 353–364.
2. Betzel, R. F. & Bassett, D. S. (2017) Multi-scale brain networks. *NeuroImage*, **160**, 73–83.
3. Sporns, O., Tononi, G. & Kötter, R. (2005) The human connectome: A structural description of the human brain. *PLoS Comput. Biol.*, **1**, e42.
4. Sporns, O. (2013) Structure and function of complex brain networks. *Dialogues Clin. Neurosci.*, **15**, 247–262.
5. Sporns, O. (2015) Cerebral cartography and connectomics. *Philos. Trans. R. Soc. Lond. B Biol. Sci.*, **370**, 20140173.
6. Sporns, O. & Betzel, R. F. (2015) Modular brain networks. *Annu. Rev. Psychol.*, **67**, 613–640.
7. Papo, D., Buldú, J. M., Boccaletti, S. & Bullmore, E. T. (2014) Complex network theory and the brain. *Philos. Trans. R. Soc. Lond. B Biol. Sci.*, **369**, 20130520.
8. Petersen, S. E. & Sporns, O. (2015) Brain networks and cognitive architectures. *Neuron*, **88**, 207–219.
9. Supekar, K., Menon, V., Rubin, D., Musen, M. & Greicius, M. D. (2008) Network analysis of intrinsic functional brain connectivity in Alzheimer's disease. *PLoS Comput. Biol.*, **4**, e1000100.
10. Dichter, G. S. (2012) Functional magnetic resonance imaging of autism spectrum disorders. *Dialogues Clin. Neurosci.*, **14**, 319–351.
11. Lynall, M.-E., Bassett, D. S., Kerwin, R., McKenna, P. J., Kitzbichler, M., Muller, U. & Bullmore, E. T. (2010) Functional connectivity and brain networks in schizophrenia. *J. Neurosci.*, **30**, 9477–9487.
12. van den Heuvel, M. P., Sporns, O., Collin, G., Scheewe, T., Mandl, R. C. W., Cahn, W., Goñi, J., Hulshoff Pol, H. E. & Kahn, R. S. (2013) Abnormal rich club organization and functional brain dynamics in schizophrenia. *JAMA Psychiatry*, **70**, 783–792.
13. Hadley, J. A., Kraguljac, N. V., White, D. M., Ver Hoef, L., Tabora, J. & Lahti, A. C. (2016) Change in brain network topology as a function of treatment response in schizophrenia: A longitudinal resting-state fMRI study using graph theory. *npj Schizophr.* **2**, 16014.
14. Greicius, M. (2008) Resting-state functional connectivity in neuropsychiatric disorders. *Curr. Opin. Neurol.*, **21**, 424–430.
15. Kendell, R. & Jablensky, A. (2013) Distinguishing between the validity and utility of psychiatric diagnoses. *Am. J. Psychiatry*, **160**, 4–12.
16. Kay, S. R., Fiszbein, A. & Opler, L. A. (1987) The positive and negative syndrome scale (PANSS) for schizophrenia. *Schizophr. Bull.*, **13**, 261–276.
17. Dold, M., Tardy, M., Samara, M. T., Li, C., Kasper, S. & Leucht, S. (2016) Are all first-generation antipsychotics equally effective in treating schizophrenia? A meta-analysis of randomised, haloperidol-controlled trials. *World J. Biol. Psychiatry*, **17**, 210–220.
18. Leucht, S., Komossa, K., Rummel-Kluge, C., Corves, C., Hunger, H., Schmid, F., Asenjo Lobos, C., Schwarz, S. & Davis, J. M. (2009) A meta-analysis of head-to-head comparisons of second-generation antipsychotics in the treatment of schizophrenia. *Am. J. Psychiatry*, **166**, 152–163.
19. Tuplin, E. W. & Holahan, M. R. (2017) Aripiprazole, a drug that displays partial agonism and functional selectivity. *Curr. Neuropharmacol.*, **15**, 1192–1207.
20. Jones, P. B., Barnes, T. R., Davies, L., Dunn, G., Lloyd, H., Hayhurst, K. P., Murray, R. M., Markwick, A. & Lewis, S. W. (2006) Randomized controlled trial of the effect on quality of life of second- vs first-generation antipsychotic drugs in schizophrenia: Cost Utility of the Latest Antipsychotic drugs in Schizophrenia Study (CUtLASS 1). *Arch. Gen. Psychiatry*, **63**, 1079–1087.
21. Naber, D. & Lambert, M. (2009) The CATIE and CUtLASS studies in schizophrenia: Results and implications for clinicians. *CNS Drugs*, **23**, 649–659.

22. Marder, S. R., McQuade, R. D., Stock, E., Kaplita, S., Marcus, R., Safferman, A. Z., Saha, A., Ali, M. & Iwamoto, T. (2003) Aripiprazole in the treatment of schizophrenia: Safety and tolerability in short-term, placebo-controlled trials. *Schizophr. Res.*, **61**, 123–136.

23. Shiloh, R., Zemishlany, Z., Aizenberg, D., Radwan, M., Schwartz, B., Dorfman-Etrog, P., Modai, I., Khaikin, M. & Weizman, A. (1997) Sulpiride augmentation in people with schizophrenia partially responsive to clozapine. A double-blind, placebo-controlled study. *Br. J. Psychiatry*, **171**, 569–573.

24. Alexander-Bloch, A., Lambiotte, R., Roberts, B., Giedd, J., Gogtay, N. & Bullmore, E. T. (2012) The discovery of population differences in network community structure: New methods and applications to brain functional networks in schizophrenia. *NeuroImage*, **59**, 3889–3900.

25. Porter, M. A., Onnela, J.-P. & Mucha, P. J. (2009) Communities in networks. *Notices Am. Math. Soc.*, **56**, 1082–1097, 1164–1166.

26. Fortunato, S. & Hric, D. (2016) Community detection in networks: A user guide. *Phys. Rep.*, **659**, 1–44.

27. Bassett, D. S., Wymbs, N. F., Rombach, M. P., Porter, M. A., Mucha, P. J. & Grafton, S. T. (2013) Task-based core-periphery organization of human brain dynamics. *PLoS Comput. Biol.*, **9**, e1003171.

28. Lui, S., Li, T., Deng, W., Jiang, L., Wu, Q., Tang, H., Yue, Q., Huang, X., Raymond, R. C., Collier, D. A. & Meda, S. A. (2010) Short-term effects of antipsychotic treatment on cerebral function in drug-naive first-episode schizophrenia revealed by 'resting state' functional magnetic resonance imaging. *Arch. Gen. Psychiatry*, **67**, 783–792.

29. Towlson, E. K., Vértes, P. E., Müller, U. & Ahnert, S. E. (2018) Brain networks reveal the effects of antipsychotic drugs on schizophrenia patients and controls. ArXiv:1806.00128.

30. Onnela, J.-P., Fenn, D. J., Reid, S., Porter, M. A., Mucha, P. J., Fricker, M. D. & Jones, N. S. (2012) Taxonomies of networks from community structure. *Phys. Rev. E*, 86, 036104.

31. Zalesky, A., Fornito, A., Harding, I. H., Cocchi, L., Yücel, M., Pantelis, C. & Bullmore, E. T. (2010) Whole-brain anatomical networks: Does the choice of nodes matter? *NeuroImage*, **50**, 970–983.

32. Power, J. D., Barnes, K. A., Snyder, A. Z., Schlaggar, B. L. & Petersen, S. E. (2012) Spurious but systematic correlations in functional connectivity MRI networks arise from subject motion. *NeuroImage*, **59**, 2142–2154.

33. Satterthwaite, T. D., Wolf, D. H., Loughead, J., Ruparel, K., Elliott, M. A., Hakonarson, H., Gur, R. C. & Gur, R. E. (2012) Impact of in-scanner head motion on multiple measures of functional connectivity: Relevance for studies of neurodevelopment in youth. *NeuroImage*, **60**, 623–632.

34. Van Dijk, K. R., Sabuncu, M. R. & Buckner, R. L. (2012) The influence of head motion on intrinsic functional connectivity MRI. *NeuroImage*, **59**, 431–438.

35. Patel, A. X., Kundu, P., Rubinov, M., Jones, P. S., Vértes, P. E., Ersche, K. D., Suckling, J. & Bullmore, E. T. (2014) A wavelet method for modeling and despiking motion artifacts from resting-state fMRI time series. *NeuroImage*, **95**, 287–304.

36. Suckling, J., Long, C., Triantafyllou, C., Brammer, M. & Bullmore, E. T. (2006) Variable precision registration via wavelets: Optimal spatial scales for inter-subject registration of functional MRI. *NeuroImage*, **31**, 197–208.

37. Zalesky, A., Fornito, A., Egan, G. F., Pantelis, C. & Bullmore, E. T. (2012) The relationship between regional and inter-regional functional connectivity deficits in schizophrenia. *Hum. Brain Mapp.*, **33**, 2535–2549.

38. Percival, D. B. & Walden, A. T. (2000) *Wavelet Methods for Time Series Analysis*. Cambridge, UK: Cambridge University Press.

39. Cordes, D., Haughton, V. M., Arfanakis, K., Wendt, G. J., Turski, P. A., Moritz, C. H., Quigley, M. A. & Meyerand, M. E. (2000) Mapping functionally related regions of brain with functional connectivity MR imaging. *Am. J. Neuroradiol.*, **21**, 1636–1644.

40. Zhan, L., Jenkins, L. M., Wolfson, O. E., GadElkarim, J. J., Nocito, K., Thompson, P. M., Ajilore, O. A., Chung, M. K. & Leow, A. D. (2017) The significance of negative correlations in brain connectivity. *J. Comp. Neurol.*, **525**, 3251–3265.

41. Liu, Y., Liang, M., Zhou, Y., He, Y., Hao, Y., Song, M., Yu, C., Liu, H., Liu, Z. & Jiang, T. (2008) Disrupted small-world networks in schizophrenia. *Brain*, **131**, 945–961.

42. He, H., Sui, J., Yu, Q., Turner, J. A., Ho, B.-C., Sponheim, S. R., Manoach, D. S., Clark, V. P. & Calhoun, V. D. (2012) Altered small-world brain networks in schizophrenia patients during working memory performance. *PLoS One*, **7**, e38195.

43. Achard, S., Salvador, R., Whitcher, B., Suckling, J. & Bullmore, E. T. (2006) A resilient, low-frequency, small-world human brain functional network with highly connected association cortical hubs. *J. Neurosci.*, **26**, 63–72.

44. Saramäki, J., Kivelä, M., Onnela, J.-P., Kaski, K. & Kertész, J. (2007) Generalizations of the clustering coefficient to weighted complex networks. *Phys. Rev. E*, **75**, 027105.

45. Newman, M. E. J. & Girvan, M. (2004) Finding and evaluating community structure in networks. *Phys. Rev. E*, **69**, 026113.

46. Newman, M. E. J. (2006) Finding community structure in networks using the eigenvectors of matrices. *Phys. Rev. E*, **74**, 036104.

47. Blondel, V. D., Guillaume, J.-L., Lambiotte, R. & Lefebvre, E. (2008) Fast unfolding of communities in large networks. *J. Stat. Mech. Theory Exp.*, P10008.

48. Bazzi, M., Porter, M. A., Williams, S., McDonald, M., Fenn, D. J. & Howison, S. D. (2016) Community detection in temporal multilayer networks, with an application to correlation networks. *Multiscale Model. Simul.*, **14**, 1–41.

49. Reichardt, J. & Bornholdt, S. (2006) Statistical mechanics of community detection. *Phys. Rev. E*, **74**, 016110.

50. Lee, S. H., Fricker, M. D. & Porter, M. A. (2017) Mesoscale analyses of fungal networks as an approach for quantifying phenotypic traits. *J. Complex Netw.*, **5**, 145–159.

51. Schütze, H., Manning, C. D. & Raghavan, P. (2009) *An Introduction to Information Retrieval*. Cambridge, UK: Cambridge University Press.

52. Eklund, A., Nichols, T. E. & Knutsson, H. (2016) Cluster failure: Why fMRI inferences for spatial extent have inflated false-positive rates. *Proc. Natl. Acad. Sci. U.S.A.*, **113**, 7900–7905.

53. Kopell, N. J., Gritton, H. J., Whittington, M. A. & Kramer, M. A. (2014) Beyond the connectome: The dynome. *Neuron*, **83**, 1319–1328.

54. Buldú, J. M. & Porter, M. A. (2018) Frequency-based brain networks: From a multiplex network to a full multilayer description. *Netw. Neurosci.*, **2**, 418–441.

A. Appendix: Metric properties of d_1

In this appendix, we state and prove a theorem on the metric properties of d_1 (which we defined in Eq. (3)) that is slightly more general than the one that we used in the main text. The result in the main text follows from it as a trivial corollary.

Theorem 1 Let $\mathcal{S}_n(E)$ be the set of $n \times n$ square matrices with entries of 0 or 1 (i.e., 'binary matrices'), where the number E of 1 entries satisfies $E < n^2$. Let $\mathbf{A}, \mathbf{B} \in \mathcal{S}_n(E)$ be two arbitrary elements of the set. Consider the function d_1 defined by

$$d_1 : \mathcal{S}_n(E) \times \mathcal{S}_n(E) \to [0,1], \quad d_1(\mathbf{A},\mathbf{B}) = 1 - \frac{1}{E}\sum_{i=1}^{n}\sum_{j=1}^{n} A_{ij}B_{ij}\,. \tag{A.1}$$

The function d_1 is a metric.

The definition in (A.1) for d_1 is slightly more general than the one in Eq. (3), as here we are not assuming that (1) $\mathbf{A}$ and $\mathbf{B}$ are symmetric or that (2) there are no 1 entries in the diagonal (so E is the

number of 1 entries). In the main text, we imposed some restrictions on E that are not present here: we used E to denote the number of edges in an associated network, so for Eq. (3) (which is designed to deal with unweighted, undirected adjacency matrices with no self-loops), one needs either to restrict to the case in which there are no 1 entries in the main diagonal and then do the relabelling $E \to E/2$ or to relabel the summation indices with $\sum_{i=1}^{n}\sum_{j=1}^{n} \to \sum_{i>j}$. The theorem that we used in the main text is thus a special case of Theorem 1.

Proof. To prove that d_1 is a metric, we need to prove four properties: non-negativity, identity of indiscernibles, symmetry and the triangle inequality. The first three properties are satisfied trivially:

(1) Non-negativity: By construction, $\sum_{i=1}^{n}\sum_{j=1}^{n} A_{ij}B_{ij} \leq E$, so $d_1(\mathbf{A},\mathbf{B}) \geq 0$.

(2) Identity of indiscernibles: $d_1(\mathbf{A},\mathbf{B}) = 0 \Leftrightarrow \sum_{i=1}^{n}\sum_{j=1}^{n} A_{ij}B_{ij} = E$. However, by definition, the matrices are binary and have E entries with the value 1, so $\sum_{i=1}^{n}\sum_{j=1}^{n} A_{ij}B_{ij} = E \Leftrightarrow \mathbf{A} = \mathbf{B}$.

(3) Symmetry: This arises trivially from the commutative property of the scalar product: $A_{ij}B_{ij} = B_{ij}A_{ij}$.

To prove the fourth property (the triangle inequality), we need to show that

$$\text{for all } \mathbf{A},\mathbf{B},\mathbf{C} \in \mathcal{S}_n(E)\,, \quad d_1(\mathbf{A},\mathbf{B}) + d_1(\mathbf{B},\mathbf{C}) \geq d_1(\mathbf{A},\mathbf{C})\,. \tag{A.2}$$

This part is more subtle, and we need to break the proof into a few steps. We start by defining a *matrix δ-perturbation*.

DEFINITION 1 (MATRIX δ-PERTURBATION). Let $\mathbf{A} \in \mathcal{S}_n(E)$, and let δ be a positive integer such that $0 < \delta < E$. The matrix $\tilde{\mathbf{A}}^{(\delta)}$ is a δ-perturbation of $\mathbf{A}$ if $\tilde{\mathbf{A}}^{(\delta)}$ is constructed by taking $\mathbf{A}$ and changing the position of δ of the 1 entries.

To illustrate this definition, we show an example of a matrix and a 1-perturbation of that matrix in $S_3(3)$:

$$\mathbf{Z} = \begin{bmatrix} 1 & 0 & 0 \\ 1 & 0 & 0 \\ 0 & 1 & 0 \end{bmatrix}, \quad \tilde{\mathbf{Z}}^{(1)} = \begin{bmatrix} 0 & 0 & 1 \\ 1 & 0 & 0 \\ 0 & 1 & 0 \end{bmatrix}. \tag{A.3}$$

It is clearly the case that $\tilde{\mathbf{A}}^{(\delta)} \in \mathcal{S}_n(E)$. It is also true that

$$\sum_{i=1}^{n}\sum_{j=1}^{n} A_{ij}\tilde{A}_{ij}^{(\delta)} = E - \delta \;\Rightarrow\; d_1(\tilde{\mathbf{A}}^{(\delta)},\mathbf{A}) = \delta/E\,.$$

Starting from an arbitrary element of $\mathcal{S}_n(E)$, one can reach any other element by applying an appropriate δ-perturbation. Therefore, equipped with the δ-perturbation, $\mathcal{S}_n(E)$ is a unary system. This property is important for guaranteeing completeness.

To prove Eq. (A.2), it is equivalent to prove that

$$\text{for all } \mathbf{A},\mathbf{B},\mathbf{C} \in \mathcal{S}_n(E)\,, \quad \mathcal{X} := \sum_{i=1}^{n}\sum_{j=1}^{n}(A_{ij}B_{ij} + B_{ij}C_{ij} - A_{ij}C_{ij}) \leq E\,.$$

We are ready to prove this latter inequality. We start with a degenerate case. Consider an arbitrary $\mathbf{A} \in \mathcal{S}_n(E)$ and set $\mathbf{A} = \mathbf{B} = \mathbf{C}$; in this case, $\mathcal{X} = \sum_{i=1}^{n} \sum_{j=1}^{n} A_{ij} A_{ij} = E \leq E$.

To generate all possible triples $\{\mathbf{A}, \mathbf{B}, \mathbf{C}\}$, without loss of generality, we now consider an arbitrary (but fixed) $\mathbf{A} \in \mathcal{S}_n(E)$; and we use δ-perturbations to generate all instances of $\mathbf{B}$ and $\mathbf{C}$. That is,

$$\mathbf{B} := \tilde{\mathbf{A}}^{(\delta_b)}, \mathbf{C} := \tilde{\mathbf{A}}^{(\delta_c)}, \text{ with } \delta_b, \delta_c \geq 0 .$$

All possible triples can be expressed in this form.

Let's evaluate $\mathcal{X}$. The first term is

$$\sum_{i=1}^{n} \sum_{j=1}^{n} A_{ij} B_{ij} = \sum_{i=1}^{n} \sum_{j=1}^{n} A_{ij} \tilde{A}_{ij}^{(\delta_b)} = E - \delta_b ;$$

the second term is

$$\sum_{i=1}^{n} \sum_{j=1}^{n} B_{ij} C_{ij} = \sum_{i=1}^{n} \sum_{j=1}^{n} \tilde{A}_{ij}^{(\delta_b)} \tilde{A}_{ij}^{(\delta_c)} ;$$

and the third term is

$$\sum_{i=1}^{n} \sum_{j=1}^{n} A_{ij} C_{ij} = \sum_{i=1}^{n} \sum_{j=1}^{n} A_{ij} \tilde{A}_{ij}^{(\delta_c)} = E - \delta_c .$$

We need to separately consider the cases in which two matrices experience the same perturbation or different perturbations. In the usual case, $\delta_b \neq \delta_c$ (i.e., the perturbations are different), so there is at least an offset of $|\delta_b - \delta_c|$. Consequently,

$$\sum_{i=1}^{n} \sum_{j=1}^{n} \tilde{A}_{ij}^{(\delta_b)} \tilde{A}_{ij}^{(\delta_c)} \leq E - |\delta_b - \delta_c| . \tag{A.4}$$

If, however, $\delta_b = \delta_c$ (i.e., both δ-perturbations are the same), the right-hand side of Eq. (A.4) is instead given by E.

Altogether, this yields the following bound:

$$\mathcal{X} \leq E - \delta_b + E - |\delta_b - \delta_c| - E + \delta_c = E + (\delta_c - \delta_b) - |\delta_b - \delta_c| .$$

Three possibilities emerge:

(1) If $\delta_b = \delta_c$, then $\mathcal{X} \leq E$.

(2) If $\delta_b < \delta_c$, then $|\delta_b - \delta_c| = \delta_c - \delta_b$, so $\mathcal{X} \leq E$.

(3) If $\delta_b > \delta_c$, then $|\delta_b - \delta_c| = \delta_b - \delta_c$, so $\mathcal{X} \leq E + 2(\delta_c - \delta_b) < E$.

This concludes the proof. □

B. Appendix: An urn-type null model

We now examine an urn-type null model to assess the statistical significance of some of our calculations. In Section 4.3, we discussed the notion of purity and used it to quantify the clustering quality in three dendrograms. Our data set is small, so we cannot rule out the possibility that the observed clustering may be contaminated by statistical artefacts or finite-size effects. We thus construct an urn-type null model to assess the likelihood that the observed amount of clustering arises from chance, and we apply it to examine the results of the 'controls versus patients under Aripiprazole' dendrogram (which we labelled as case A in Fig. 8 of Section 4.3). Cutting the dendrogram at the level at which purity peaks yields two communities (each with 10 subjects) and a purity of 19/20. To compute the probability $\mathbb{P}$ that this occurred by chance, we first enumerate all possible partitions. The number Z of different configurations for partitioning the 11 controls and 9 patients into two groups of 10 individuals is

$$Z = 2\sum_{k=0}^{4}\binom{11}{10-k}\binom{9}{k} = 184756\,.$$

There are five possible events:

- Event (E1): There are 10 controls in one urn, and the other urn has 1 control and 9 patients. (This corresponds to case A of controls versus patients under Aripiprazole.) The purity in this case is 19/20, and the probability that this event occurs by chance is

$$\mathbb{P}_{\mathrm{E1}} = \frac{2}{Z}\binom{11}{10} = \frac{1}{8398} \approx 10^{-4}\,.$$

  That is, this event would occur randomly with a probability 0.0001, a seemingly very unlikely event. For completeness, we also give the estimated probabilities of the other events. We write $\kappa C + \lambda P$ to denote a set with κ controls and λ patients. The probabilities are as follows:

- Event (E2): $9C + 1P$ is in one urn, and $2C + 8P$ is in the other (purity 17/20), so

$$\mathbb{P}_{\mathrm{E2}} = \frac{2}{Z}\binom{11}{9}\binom{9}{1} = \frac{45}{8398} \approx 0.0053\,.$$

- Event (E3): $8C + 2P$ is in one urn, and $3C + 7P$ is in the other (purity 15/20), so

$$\mathbb{P}_{\mathrm{E3}} = \frac{2}{Z}\binom{11}{8}\binom{9}{2} = \frac{270}{4199} \approx 0.064\,.$$

- Event (E4): $7C + 3P$ is in one urn, and $4C + 6P$ is in the other (purity 13/20), so

$$\mathbb{P}_{\mathrm{E4}} = \frac{2}{Z}\binom{11}{7}\binom{9}{3} = \frac{1260}{4199} \approx 0.3\,.$$

- Event (E5): $6C + 4P$ is in one urn, and $5C + 5P$ is in the other (purity 11/20), so

$$\mathbb{P}_{\mathrm{E5}} = \frac{2}{Z}\binom{11}{6}\binom{9}{4} = \frac{2646}{4199} \approx 0.63\,.$$

C. Appendix: Network component sizes

As we discussed in Section 3.2, half of our networks (30 of 60) consist of two or more components after thresholding. However, even in these cases, the LCC of each network includes almost the entire network. In Table C1, we show the number of components and component sizes for each of the 60 networks.

TABLE C1 *Number of components and component sizes of each of the 60 networks. (We denote treatment under Aripiprazole by 'A', treatment under Sulpiride by 'S' and treatment under placebo by 'P'.)*

Subject	*Number of components*	*Component sizes*
Control 1 (A)	6	{293,1,1,1,1,1}
Control 3 (A)	4	{295,1,1,1}
Control 4 (A)	5	{293,2,1,1,1}
Control 5 (A)	20	{268,6,5,2,2,1,1,1,1,1,1,1,1,1,1,1,1,1,1,1}
Control 6 (A)	2	{297,1}
Control 7 (A)	3	{296,1,1}
Control 9 (A)	4	{295,1,1,1}
Control 11 (A)	2	{297,1}
Control 12 (A)	6	{292,2,1,1,1,1}
Control 13 (A)	6	{292,2,1,1,1,1}
Control 15 (A)	2	{297,1}
Control 1 (P)	1	298
Control 3 (P)	2	{297,1}
Control 4 (P)	1	298
Control 5 (P)	2	{297,1}
Control 6 (P)	5	{289,3,3,2,1}
Control 7 (P)	4	{295,1,1,1}
Control 9 (P)	2	{297,1}
Control 11 (P)	1	298
Control 12 (P)	4	{294,2,1,1}
Control 13 (P)	4	{295,1,1,1}
Control 15 (P)	1	298
Control 1 (S)	1	298
Control 3 (S)	2	{297,1}
Control 4 (S)	1	298
Control 5 (S)	1	298
Control 6 (S)	3	{296,1,1}
Control 7 (S)	1	298
Control 9 (S)	1	298
Control 11 (S)	2	{297,1}
Control 12 (S)	1	298
Control 13 (S)	3	{296,1,1}
Control 15 (S)	1	298

TABLE C1 *Continued*

Subject	*Number of components*	*Component sizes*
Patient 1 (A)	2	{297,1}
Patient 2 (A)	1	298
Patient 4 (A)	1	298
Patient 6 (A)	1	298
Patient 7 (A)	2	{297,1}
Patient 8 (A)	7	{291,2,1,1,1,1,1}
Patient 9 (A)	1	298
Patient 10 (A)	1	298
Patient 12 (A)	1	298
Patient 1 (P)	1	298
Patient 2 (P)	1	298
Patient 4 (P)	1	298
Patient 6 (P)	1	298
Patient 7 (P)	2	{297,1}
Patient 8 (P)	7	{292,1,1,1,1,1,1}
Patient 9 (P)	1	298
Patient 10 (P)	3	{296,1,1}
Patient 12 (P)	1	298
Patient 1 (S)	1	298
Patient 2 (S)	2	{297,1}
Patient 4 (S)	1	298
Patient 6 (S)	1	298
Patient 7 (S)	1	298
Patient 8 (S)	5	{294,1,1,1,1}
Patient 9 (S)	1	298
Patient 10 (S)	1	298
Patient 12 (S)	1	298